Cell Communication and Signaling

RESEARCH

Open Access

Gasdermin D promotes development of intestinal tumors through regulating IL-1β release and gut microbiota composition

Hanchao Gao[1*†], Weilong Li[1†], Shi Xu[2†], Zigan Xu[1], Wenjun Hu[3], Litao Pan[4], Kewang Luo[5], Ting Xie[6], Yeye Yu[6], Huimin Sun[1], Liwen Huang[1], Peishan Chen[1], Jinmei Wu[1], Dexing Yang[1], Lian Li[7], Shaodong Luan[1*], Mengtao Cao[8*] and Pengfei Chen[9*]

Abstract

The interplay between gut microbiota and host is crucial for maintaining host health. When this balance is broken, various diseases can arise, including colorectal cancer (CRC). However, the mechanism by which gut microbiota and host interactions mediate CRC development remains unclear. Here, we found that Gasdermin D (GSDMD), an inflammasome effector responsible for forming membrane pores to mediate cell pyroptosis, was upregulated in both human and mouse intestinal tumor samples. GSDMD deficiency significantly suppressed intestinal tumor development in $Apc^{min/+}$ mice, a spontaneous CRC mouse model. $Apc^{min/+}Gsdmd^{-/-}$ mice exhibited reduced IL-1β release in the intestine, and the administration of recombinant mouse IL-1β partially restored intestinal tumor development in $Apc^{min/+}Gsdmd^{-/-}$ mice. Moreover, 16s rRNA sequencing showed a substantial increase in *Lactobacillus* abundance in the feces of $Apc^{min/+}Gsdmd^{-/-}$ mice compared to $Apc^{min/+}$ mice. Concurrently, Kynurenine (Kyn), a metabolite derived from host tryptophan (Trp) metabolism, was significantly decreased in the feces of $Apc^{min/+}Gsdmd^{-/-}$ mice, as shown by metabolite analysis. Additionally, Kyn levels were inversely correlated with *Lactobacillus* abundance. Furthermore, the administration of exogenous Kyn also promoted intestinal tumor development in $Apc^{min/+}Gsdmd^{-/-}$ mice. Thus, GSDMD promotes spontaneous CRC development through increasing IL-1β release and Kyn production. Our data suggest an association between GSDMD, gut microbiota, the host Trp/Kyn pathway, and CRC development.

Keywords Colon cancer, GSDMD, Gut microbiota, Metabolite

[†]Hanchao Gao, Weilong Li and Shi Xu contributed equally to this work.

*Correspondence:
Hanchao Gao
hcgao@foxmail.com
Shaodong Luan
szkidney3@163.com
Mengtao Cao
cmtbnu@163.com
Pengfei Chen
pfchen@sibs.ac.cn

Full list of author information is available at the end of the article

Introduction

Colorectal cancer (CRC) is the third most common malignancy and one of the leading causes of death worldwide [1]. The adenomatous polyposis coli (*Apc*) gene functions as a tumor suppressor, and its loss leads to the development of intestinal tumor. The $Apc^{min/+}$ mice strain, which harbors an inactivating mutation in the *Apc* gene, is a widely used spontaneous mouse model for CRC [2, 3]. This model is clinically relevant because the intravillus adenomas in $Apc^{min/+}$ mice resemble those found in the duodenum of patients with familial adenomatous polyposis (FAP) [4].

CRC is closely linked to gut microbiota and inflammation [5]. The interaction between gut microbiota and the host is critical for maintaining intestinal homeostasis. When the balance is disrupted, aberrant inflammation and metabolic dysregulation may trigger diseases such as CRC. *Lactobacillus* is commonly observed to decrease in CRC cases and is considered a probiotic that may help prevent CRC development. However, the precise mechanisms by which *Lactobacillus* suppresses CRC development are not yet fully understood [5].

The inflammasome is an intracellular multiprotein complex responsible for the maturation of interleukin-1β (IL-1β) and IL-18, as well as the induction of cell pyroptosis [6]. While the primary function of the inflammasome is to protect the host from pathogenic infections, chronic activation leads to pathological inflammation, thereby exacerbating CRC progression. Several studies have demonstrated that the inflammasome pathway is critical in CRC development [7]. Major inflammasome components, such as NLRP3, NLRP1b, NLRC4, NLRP6, Pyrin, ASC, AIM2, Caspase 1, Caspase 11, IL-18, and IL-1β, play important roles in CRC development [1, 8]. On the other hand, some reports suggest that the inflammasome can suppress CRC development through IL-18 dependent and independent mechanisms [8]. IL-18 has been shown to suppress CRC development by promoting epithelial cells regeneration and inhibiting the expression of IL-22 binding protein (IL-22 bp) and IL-22 receptor (IL-22R). Conversely, IL-1β is widely recognized for its role in promoting CRC by enhancing tumor cell proliferation and shaping the tumor microenvironment [9–12].

GSDMD is a novel inflammasome effector which triggers the release of mature IL-1β and IL-18, and promotes cell pyroptosis [13, 14]. Upon activation by damage-associated molecular patterns (DAMPs), GSDMD is cleaved by Caspase 1/11 in mice or Caspase 1/4/5 in humans, yielding the active N-terminal domain (GSDMD-N) and the C-terminal domain (GSDMD-C). The GSDMD-N fragment translocates to the plasma membrane, mediating cell pyroptosis and the release of mature IL-1β and IL-18 [15]. In canonical inflammasome, Caspase 1 cleaves GSDMD to initiate cell pyroptosis, while in noncanonical inflammasome, lipopolysaccharide (LPS) directly activates Caspase 4/5/11 in cytoplasm, which in turn cleaves GSDMD to mediate pyroptosis [16]. GSDMD has been shown to enhance chemotherapy drug-induced cell death in colon cancer [17, 18]. However, its role in spontaneous colon cancer remains controversial. One study showed that GSDMD repressed inflammation-induced CRC progression [19], while another study found that a point mutation in leucine-rich repeat kinase 2 (LRRK2), G2019S, promoted inflammation-associated CRC through LRRK2-GSDMD-mediated gut inflammation [20].

Kynurenine (Kyn), a metabolite derived from tryptophan, is considered to be an oncometabolite in CRC [21]. Kyn levels are elevated in colon cancer tissues compared to healthy samples [22, 23]. Kyn facilitates CRC development through several mechanisms, including the promotion of regulatory T cell (Treg) differentiation [22] and $CD8^+$ T cell exhaustion [24], increased proliferation of colon cancer cells, and the suppression of apoptosis [23, 25].

In the study, we found that GSDMD was upregulated in intestinal cancer and promoted IL-1β-dependent spontaneous intestinal cancer development. GSDMD deficiency led to an increased abundance of *Lactobacillus* and a decreased Kyn levels in the feces of spontaneous intestinal cancer mice. Kyn, a metabolite of tryptophan derived from the host rather than from bacteria, was shown to restore intestinal tumor development in $Apc^{min/+}Gsdmd^{-/-}$ mice. These findings suggest that GSDMD promotes CRC development through increasing IL-1β release and Kyn production. Additionally, our results indicate that GSDMD deficiency alters the gut microbiota composition, which is associated with changes in the host Trp/Kyn metabolic pathway during CRC development.

Materials and methods

Human colorectal cancer tissue microarray

A commercial tissue microarray (HColA160CS01) was purchased from Shanghai Outdo Biotech (Shanghai, China). Anti-GSDMD antibody (Proteintech) was used to evaluate GSDMD expression in intestinal cancer via immunohistochemistry (IHC). Microwave heating was used for antigen retrieval in citrate buffer (pH 6.0) for 5 min. The tissue microarray was incubated with the anti-GSDMD antibody at 4°C overnight. Slides were analyzed independently by two pathologists. Staining intensity was graded from 0 (negative staining) to 3 (strong positive staining), with intermediate scores of 0.5, 1, and 2. Positive percentage scores ranged from 0 to 100%. The overall GSDMD expression score was calculated by multiplying the staining intensity by the positive percentage score.

Reagents

Anti-GSDMD antibody for immunoblot analysis was sourced from Abcam (Cambridge, UK), while the anti-GAPDH antibody was obtained from Cell Signaling Technology (Danvers, MA, US). ELISA kits for tryptophan (Trp) and kynurenine (Kyn) were purchased from Senbeijia Biotech (Nanjing, China).

Mice

Gsdmd$^{-/-}$ mice and *Apc*$^{min/+}$ mice on the C57BL/6 background were purchased from GemPharmatech (Nanjing, China). All mice were housed under specific pathogen-free conditions, and littermates from the same mouse line were bred as strict controls. *Apc*$^{min/+}$ and *Apc*$^{min/+}$*Gsdmd*$^{-/-}$ mice were sacrificed at 20 weeks of age for analysis. 8-week-old *Apc*$^{min/+}$*Gsdmd*$^{-/-}$ mice were injected intraperitoneally once per week with L-KYN (2922-83-0, Solarbio, Beijing, China) at 5 mg/kg body weight or with PBS (control mice) and sacrificed at 20 weeks for analysis. Macroscopic intestinal tumors were counted and measured with the caliper. Tumor load was calculated as the sum of all tumors' diameters present in a given mouse. All animal experiments were performed in compliance with the guide for the care and use of laboratory animals and were approved by the institutional biomedical research ethics committee of Guangdong Medical University.

Recombinant mouse IL-1β administration

Recombinant mouse IL-1β (Novoprotein, Shanghai, China) or PBS as negative control was injected into eight-week-old *Apc*$^{min/+}$ and *Apc*$^{min/+}$*Gsdmd*$^{-/-}$ mice intraperitoneally at a dose of 0.5 μg per mouse (in 200 μl sterile PBS) twice weekly, and the mice were sacrificed at 20 weeks of age for analysis.

RT-PCR

The procedure for real-time PCR has been described previously [26]. Briefly, total RNA was extracted from intestinal tumors of *Apc*$^{min/+}$, *Apc*$^{min/+}$*Gsdmd*$^{-/-}$, and IL-1β-treated *Apc*$^{min/+}$*Gsdmd*$^{-/-}$ mice, as well as from control intestinal tissues of WT and *Gsdmd*$^{-/-}$ mice using TRIzol® Reagent (Invitrogen, Shanghai, China). cDNA was synthesized with PrimeScript™ RT Master Mix (Takara Bio, Dalian, China). The levels of genes of the interest were quantified using TB Green®*Premix Ex Taq*™ (Tli RNaseH Plus) (Takara Bio). The expression levels of the genes were calculated by the $2^{-\Delta\Delta Ct}$ method and normalized to β-actin. Amplification of cDNA was performed on a ViiA 7 Real-Time PCR system (Applied Biosystems, Foster City, CA, USA) with the sequences of oligonucleotide primers listed in Supplementary Table 1.

Immunoblot analysis

The protocol for immunoblot analysis has been previously reported [27]. In brief, the tissues were lysed for 30 min in ice-cold RIPA lysis buffer supplemented with 10 mM sodium fluoride (NaF), 1 mM Na_3VO_4, 1 mM phenylmethylsulfonyl fluoride, and a complete protease inhibitor cocktail (Roche). Lysates were separated via SDS-PAGE and transferred to polyvinylidene fluoride (PVDF) membranes (Millipore, Shanghai, China). Membranes were blocked at room temperature for 1 h and incubated overnight at 4 °C with primary antibodies. After incubation with secondary antibodies at room temperature for 1 h, blots were visualized using enhanced chemiluminescence (ECL) reagents (Millipore).

Histology

Intestinal tissue was fixed in 4% paraformaldehyde (PFA) for 48 h and then embedded in paraffin wax. 5-mm sections were stained with hematoxylin-eosin (H&E). To assess cell proliferation, paraffin sections were stained using anti-Ki67 antibody (Servicebio, Wuhan, Hubei, China).

Enzyme-linked immunosorbent assay (ELISA)

To measure the protein level of IL-1β in intestinal tumors, intestinal tumors from *Apc*$^{min/+}$ and *Apc*$^{min/+}$*Gsdmd*$^{-/-}$ mice, as well as control intestinal tissues from WT and *Gsdmd*$^{-/-}$ mice were weighed and mechanically homogenized in PBS containing 1% NP-40 and a complete protease inhibitor cocktail (Roche). The protein level of IL-1β in intestine tissue homogenate was quantified using an IL-1β ELISA kit (R&D Systems, Minneapolis, MN) according to the manufacturer's instructions.

To determine the levels of Kyn and Trp in the colon, the concentrations of these metabolites in colon tissues from *Apc*$^{min/+}$ and *Apc*$^{min/+}$*Gsdmd*$^{-/-}$ mice were quantified using corresponding ELISA kits (Senbeijia, Nanjing, China), in accordance with the manufacturer's protocol.

To assess the levels of Kyn in serum and feces, eight-week-old *Apc*$^{min/+}$*Gsdmd*$^{-/-}$ mice received weekly injections of either Kyn or PBS. Two weeks later, Kyn levels in the serum and feces of these mice were measured using a Kyn ELISA kit (Senbeijia, Nanjing, China), following the manufacturer's protocol.

Flow cytometry analysis

Freshly isolated tumor tissues were chopped into small pieces and digested with 0.01% (w/v) Liberase TH (Roche, 5401151001) and 100 U/ml DNase I (Roche, 10104159001) in RPMI 1640 for 20 min at 37 °C. Cells were filtered through a 40-μm cell strainer and washed with 5 ml wash buffer (1 × PBS with 2 mM EDTA and 0.5% BSA), followed by centrifugation at 200 g for 5 min. The cells were stained with fluorescence-labeled

anti-mouse CD45 (Biolegend, 103132), anti-mouse CD4 (Biolegend, 100406), anti-mouse CD8 (Biolegend, 100712), anti-mouse Foxp3 antibodies (Biolegend, 118904) using the Foxp3/Transcription Factor Staining Buffer Set (ThermoFisher, 00-5523-00). Cells were washed, resuspended in PBS containing 1% BSA, and analyzed by BD FACS Aria II flow cytometer (Franklin Lakes, NJ, USA).

16S ribosomal RNA gene sequencing

Genomic DNA was extracted from fecal samples of 10-week-old $Apc^{min/+}$ and $Apc^{min/+}Gsdmd^{-/-}$ mice using the OMEGA Soil DNA Kit (M5635-02) (Omega Bio-Tek, Norcross, GA, USA), and stored at -20 °C for further analysis. DNA quality and quantity were assessed via agarose gel electrophoresis and NanoDrop NC2000 spectrophotometer (Thermo Fisher Scientific, Waltham, MA, USA). PCR amplification of the bacterial 16S rRNA genes V3-V4 region was performed using the forward primer 338 F (5'-ACTCCTACGGGAGGCAGCA-3') and the reverse primer 806R (5'-GGACTACHVGGGTWTCTAAT-3'). Sample-specific 7-bp barcodes were incorporated into the primers for multiplex sequencing. The PCR products were purified with Vazyme VAHTSTM DNA Clean Beads (Vazyme, Nanjing, China) and quantified using the Quant-iT PicoGreen dsDNA Assay Kit (Invitrogen, Carlsbad, CA, USA). After the individual quantification step, the PCR amplicons were pooled in equal amounts, and pair-end 2*250 bp sequencing was performed using the Illumina NovaSeq platform with NovaSeq 6000 SP Reagent Kit (500 cycles). Data analyses were mainly performed using QIIME2 and R packages (v3.2.0). Alpha diversity indices, including Chao1 richness estimator and Simpson index, were calculated using the amplicon sequence variants (ASV) table in QIIME2. Principal coordinates analysis (PCoA) was performed by QIIME2 (2019.4). Venn diagram was generated to visualize the shared and unique ASVs among samples or groups using R package "VennDiagram", based on the occurrence of ASVs across samples/groups regardless of their relative abundance (Zaura, Keijser et al. 2009). Taxa abundances at the ASV levels were statistically compared among samples or groups by MetagenomeSeq, and visualized as Manhattan plots (Zgadzaj, R et al. 2016). Linear discriminant analysis effect size (LEfSe) was performed to detect differentially abundant taxa across groups using the default parameters (Segata, Izard et al. 2011). Heatmaps were performed using R package "pheatmap".

Preparation of fecal supernatant and analysis of metabolites

Fecal samples from 10-week-old $Apc^{min/+}$ and $Apc^{min/+}Gsdmd^{-/-}$ mice were prepared for Liquid chromatography-mass spectrometry (LC-MS) at BioNovoGene (Suzhou, China). In brief, samples were vortexed for 30s in a 2 ml centrifuge tube containing 600 µl MeOH. Steel balls were added to the tubes and placed in a tissue grinder for 120s at 50 Hz. The samples were treated with ultrasound at room temperature for 10 min, and then centrifuged at 12,000×g for 10 min at 4 ℃. The supernatants were filtered with 0.22-µm membrane and transferred into the detection bottle for LC-MS detection. Samples were randomized, data acquisitions were done in one batch to eliminate system errors, and the metabolites were identified based on their molecular weight, mass spectra, and retention time. The raw data were converted to mzXML format by MSConvert in ProteoWizard software package (v3.0.8789) and processed with R XCMS (v3.12.0) for feature detection, retention time correction and alignment. Annotation of metabolite using LC-MS data was done with the Compound Discover 3.3 (Thermo Scientific, Waltham, MA, USA) and referenced to the mzCloud and HMDB database. Differently expressed metabolites between two classes of samples were conducted using a statistically significant threshold of Variable Importance in Projection (VIP) value (VIP > 1) and $p \leq 0.05$ using Student's t-test analysis. The partial least squares discriminant analysis (PLS-DA) was performed with R package ropls (v1.22.0). Heatmaps were constructed using the "pheatmap" package in R language. Kyoto Encyclopedia of Genes and Genomes (KEGG) pathway analysis and network diagram were performed with MetaboAnalyst (www.metaboanalyst.ca.). Correlated heatmaps were carried out with R package cor (v4.0.3). P value < 0.05 was set as the cut-off and activation z-scores were calculated.

Statistical analysis

GraphPad Prism Software was used to perform statistical analysis and graph development. Differences between groups were evaluated using a two-tailed Student's t-test. Correlations between GSDMD expression and clinicopathological characteristics were assessed using Fisher's exact test. Statistical significance was set at $p < 0.05$. Pearson correlation analysis was used to evaluate relationships between microbiota and metabolite data.

Results

GSDMD is upregulated in intestinal cancer

To investigate GSDMD expression in intestinal cancer, a human tissue microarray consisting of 80 colorectal cancer samples and their corresponding adjacent non-tumor specimens was analyzed for GSDMD protein levels using immunohistochemistry (IHC). Compared to adjacent non-tumor tissues, GSDMD expression was significantly elevated in intestinal cancer (Fig. 1A-E). Although GSDMD was predominantly localized in the cytoplasm (Fig. 1C), nuclear expression was detected

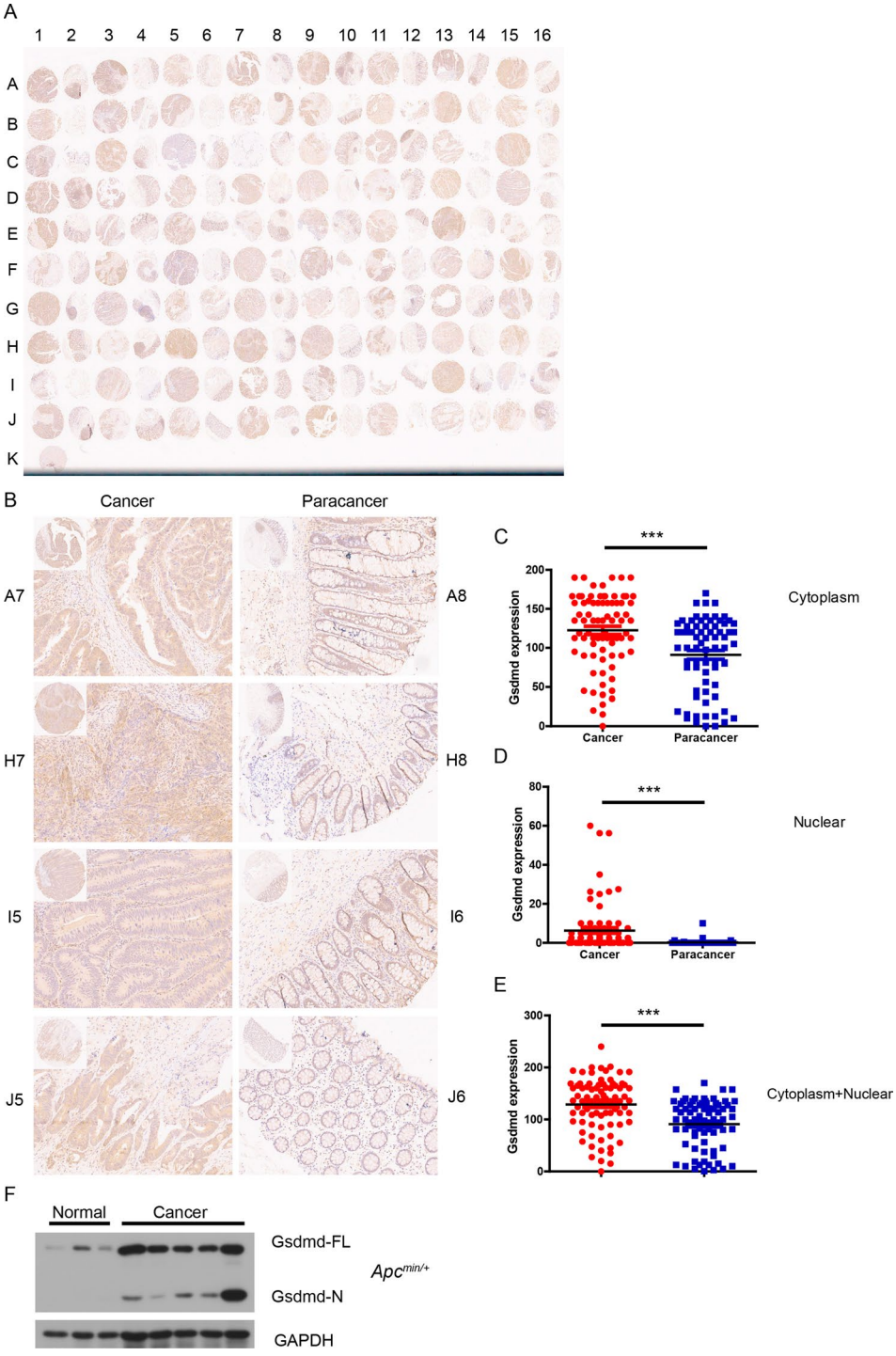

Fig. 1 GSDMD is upregulated in intestinal cancer. (**A**) IHC analysis of GSDMD protein level in a human tissue microarray, including 80 colorectal cancer and matched adjacent tumor specimens. (**B**) IHC analysis of GSDMD protein level in four colorectal cancer tissue and matched adjacent cancer tissue from (**A**) (200× magnification). (**C**-**E**) GSDMD expression score in cytoplasm (**C**), nuclear (**D**), and cytoplasm + nuclear (**E**) as calculated by multiplying the intensity and positive percentage scores according to (**A**). (**F**) Western blot analysis of GSDMD in in small intestine tumor tissue from *Apc*$^{min/+}$ mice ($n = 5$) and normal tissue from WT mice ($n = 3$). Data are representative of at least three independent experiments (mean ± SEM). ***$p < 0.001$ by Student's t test. FL means full length

in 57.5% (46/80) of tumor samples, whereas only 6.25% (5/80) of adjacent tissues exhibited GSDMD expression in the nucleus (Fig. 1D). Additionally, GSDMD expression was higher in the cytoplasm of tumor cells than in the nucleus (Fig. 1C and D). These findings suggest that GSDMD may translocate from the cytoplasm to the nucleus during the development of intestinal cancer. Fisher's exact test revealed a significant positive correlation between GSDMD expression and both tumor grade and tumor size, while no significant associations were found with patient sex, age, or tumor stage (Table 1).

In addition to human intestinal cancer, GSDMD expression was also increased in small intestinal tumor of $Apc^{min/+}$ mice, a model of spontaneous intestinal carcinogenesis (Fig. 1F). To determine whether GSDMD is activated in intestinal cancer, normal small intestine tissue and intestinal tumor tissue from $Apc^{min/+}$ mice were analyzed by immunoblot analysis, and we found that GSDMD was significantly activated in tumor tissue but not in normal tissue (Fig. 1F), suggesting that GSDMD is activated in intestinal cancer. Thus, GSDMD is upregulated in both human and mouse intestinal cancer tissues.

GSDMD promotes spontaneous intestinal cancer progression

To explore the functional role of GSDMD in spontaneous intestinal cancer, *Gsdmd*-deficient mice were crossed with $Apc^{min/+}$ mice to generate $Apc^{min/+}Gsdmd^{-/-}$ mice. Deficiency of *Gsdmd* dramatically inhibited the formation of small intestinal tumors (Fig. 2A). Histological analysis revealed a marked reduction in tumor size in $Apc^{min/+}Gsdmd^{-/-}$ mice (Fig. 2B). Both tumor number (Fig. 2C and E) and tumor load (Fig. 2D and F) were substantially reduced in the small intestines and colons of $Apc^{min/+}Gsdmd^{-/-}$ mice. Tumor size distribution analysis further demonstrated that $Apc^{min/+}Gsdmd^{-/-}$ mice had a higher proportion of smaller tumors (Fig. 2G). Consistent with severely decreased intestinal tumor development, compared to $Apc^{min/+}$ mice, the anemia and thymus atrophy were notably improved in $Apc^{min/+}Gsdmd^{-/-}$ mice (Fig. 2H and I). Additionally, $Apc^{min/+}$ mice had much larger spleen than $Apc^{min/+}Gsdmd^{-/-}$ mice (Fig. 2J). These data suggest that GSDMD is critical for the development of spontaneous intestinal cancer.

GSDMD promotes intestinal tumorigenesis via IL-1β release

IL-1β, a cytokine known to promote intestinal cancer, is released upon inflammasome activation, a process regulated by GSDMD [16]. To determine whether GSDMD influences IL-1β release during spontaneous intestinal cancer development, we compared $Apc^{min/+}$ and $Apc^{min/+}Gsdmd^{-/-}$ mice. While the mRNA levels of IL-1β were similar in tumors from both genotypes (Fig. 3A), the protein levels of IL-1β were significantly higher in tumors from $Apc^{min/+}$ mice (Fig. 3B). These findings suggest that GSDMD facilitates IL-1β release from small intestinal tumors. Some studies reported that IL-1β could promote

Table 1 Correlation between GSDMD expression and clinicopathological characteristics

	variables	GSDMD expression		total	*p* value	*r* value
		low	high			
Sex					1	0.024
	Male	30	13	43		
	Female	25	12	37		
Age (year)					0.453	-0.089
	≤ 60	17	10	27		
	> 60	38	15	53		
Grade					0.032	0.27
	I/II	48	16	64		
	III	7	9	16		
Tumor size					0.026	0.259
	≤ 4.7 cm	26	5	31		
	> 4.7 cm	29	20	49		
T stage					0.635	-0.061
	T1-T3	25	13	38		
	T4	30	12	42		
N stage					0.453	0.089
	N0	38	15	53		
	N1/N2	17	10	27		
TNM stage					0.314	0.127
	I/II	38	14	52		
	III/IV	17	11	28		

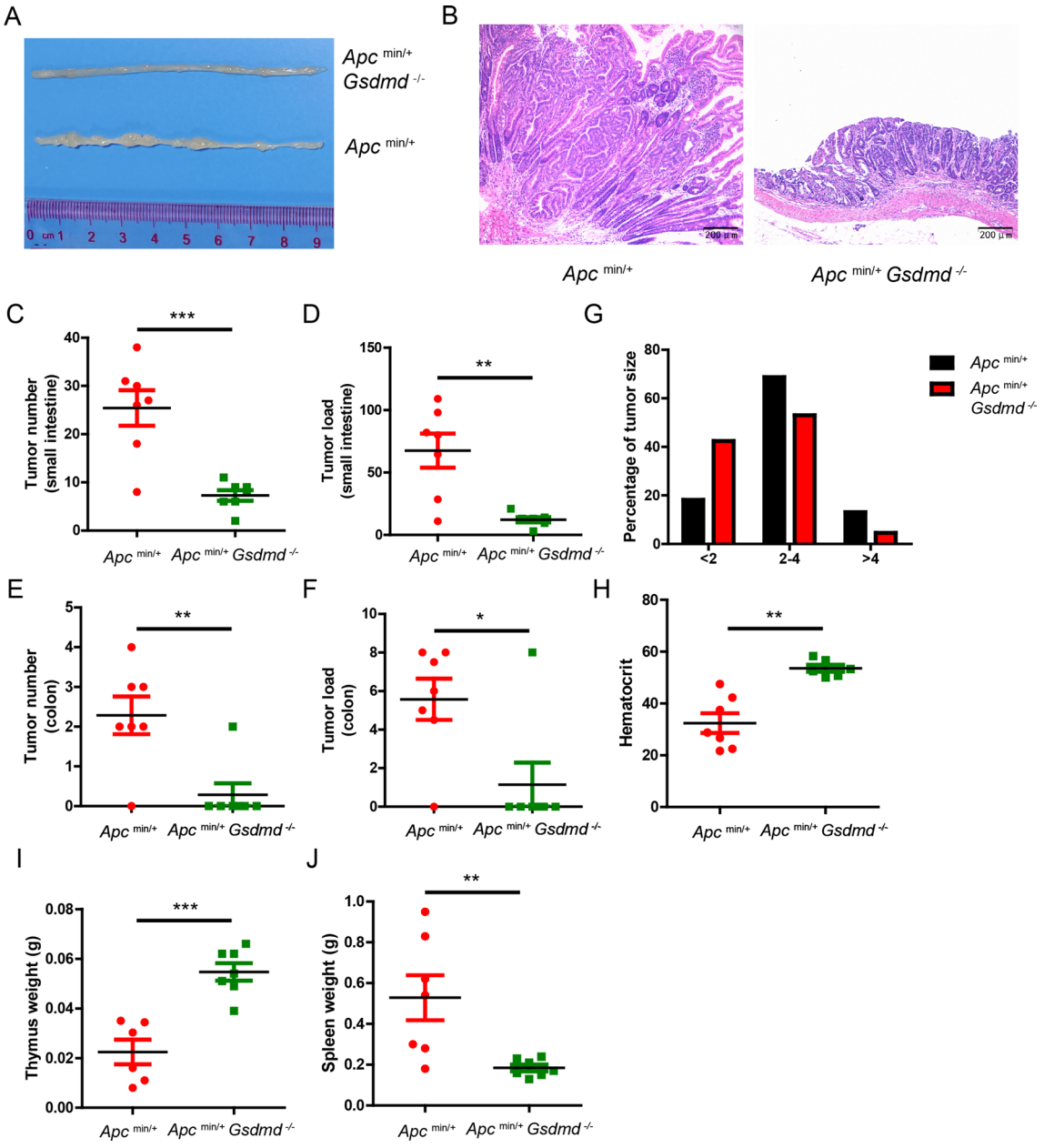

Fig. 2 Deficiency of GSDMD suppresses spontaneous intestinal cancer development. (**A**) Macroscopic view of representative small intestine from 20-week old *Apc*$^{min/+}$ and *Apc*$^{min/+}$*Gsdmd*$^{-/-}$ mice. (**B**) Hematoxylin and eosin (H&E) staining of the representative intestinal tumor from the *Apc*$^{min/+}$ and *Apc*$^{min/+}$*Gsdmd*$^{-/-}$ mice as in (**A**) (100× magnification). (**C**-**F**) Tumor number (**C** and **E**) and tumor load (**D** and **F**) from the small intestines or colons of 20-week-old *Apc*$^{min/+}$ ($n = 7$) and *Apc*$^{min/+}$*Gsdmd*$^{-/-}$ ($n = 7$) mice. (**G**) Histogram showing the size distribution of tumors from the small intestines of 20-week-old *Apc*$^{min/+}$ ($n = 7$) and *Apc*$^{min/+}$*Gsdmd*$^{-/-}$ ($n = 7$) mice. (**H**-**J**) Hematocrit (**H**), thymus weight (**I**) and spleen weight (**J**) of 20-week-old *Apc*$^{min/+}$ ($n = 6$–7) and *Apc*$^{min/+}$*Gsdmd*$^{-/-}$ ($n = 6$–7) mice. Data are representative of at least three independent experiments (mean ± SEM). *$p < 0.05$, **$p < 0.01$, ***$p < 0.001$ by Student's t test

intestinal cancer progression by promoting colon cancer growth and regulating tumor microenvironment [9–12]. Further analysis revealed that chemokine KC, HIF-1α, and pro-proliferative factors (IL-6 and CCND1) were markedly increased in *Apc*$^{min/+}$ tumors compared to *Apc*$^{min/+}$*Gsdmd*$^{-/-}$ tumors (Fig. 3C-F). The number of Ki67-positive cells, indicative of proliferating cells, was also significantly higher in *Apc*$^{min/+}$ tumors (Fig. 3G), suggesting an increased proliferation in the small intestinal tumor from *Apc*$^{min/+}$ mice. These data demonstrate that GSDMD promotes IL-1β release from intestinal tumor, and suggest that IL-1β may promote tumor progression by increasing KC, HIF-1α expression and epithelial cells proliferation.

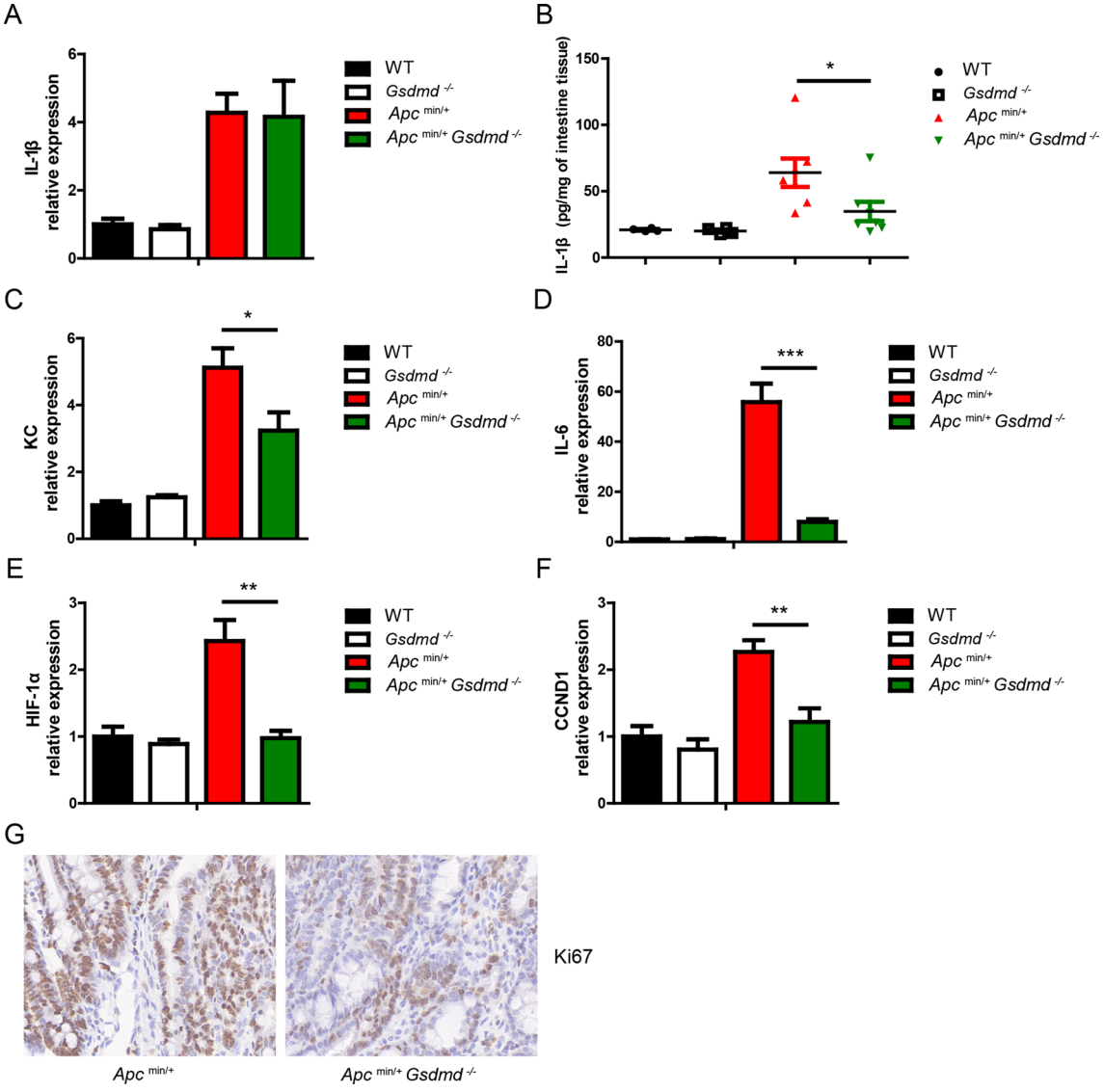

Fig. 3 Deficiency of GSDMD suppresses IL-1β release in $Apc^{min/+}$ mice. (**A**) Quantitative mRNA expression of GSDMD from small intestines of WT ($n=4$), $Gsdmd^{-/-}$ ($n=4$), $Apc^{min/+}$ ($n=7$) and $Apc^{min/+}Gsdmd^{-/-}$ ($n=6$) mice. (**B**) ELISA analysis of GSDMD protein level from small intestines of WT ($n=4$), $Gsdmd^{-/-}$ ($n=4$), $Apc^{min/+}$ ($n=7$) and $Apc^{min/+}Gsdmd^{-/-}$ ($n=7$) mice. (**C**-**F**) Quantitative mRNA expression of KC (**C**), IL-6 (**D**), HIF-1α (**E**), and CCND1 (**F**) from small intestines of WT ($n=4$), $Gsdmd^{-/-}$ ($n=4$), $Apc^{min/+}$ ($n=7$) and $Apc^{min/+}Gsdmd^{-/-}$ ($n=6$) mice. (**G**) Ki67 staining of small intestine from above mice as in (**A**) (400× magnification). Data are representative of at least three independent experiments (mean ± SEM). *$p<0.05$, **$p<0.01$, ***$p<0.001$ by Student's t test

Exogenous IL-1β partially rescues intestinal tumor formation in $Apc^{min/+}Gsdmd^{-/-}$ mice

To determine whether GSDMD promotes intestinal tumorigenesis through IL-1β, we administrated recombinant mouse IL-1β (0.5 μg) intraperitoneally twice weekly to 8-week old $Apc^{min/+}Gsdmd^{-/-}$ mice. We found that exogenous IL-1β significantly increased small intestinal tumor size in $Apc^{min/+}Gsdmd^{-/-}$ mice (Fig. 4A). The IL-1β-treated $Apc^{min/+}Gsdmd^{-/-}$ mice exhibited increased tumor number and tumor load of small intestine (Fig. 4B and C). However, both the tumor number and tumor load were lower than those in $Apc^{min/+}$ mice. Notably, exogenous IL-1β did not increase the number or load of colon tumors (Fig. 4D and E), but it did increase spleen weight (Fig. 4F) and exacerbate anemia (Fig. 4G). Tumor size distribution analysis showed that exogenous IL-1β reduced the number of small tumors in $Apc^{min/+}Gsdmd^{-/-}$ mice (Fig. 4H). The data suggest that exogenous IL-1β partially restores intestinal tumor formation in $Apc^{min/+}Gsdmd^{-/-}$ mice. Furthermore, exogenous IL-1β reinstated KC, HIF-1α, IL-6, and CCND1 expression in these mice (Figure S1A-S1D), and the number of Ki67-positive cells was also increased (Figure S1E). Together, these findings suggest that GSDMD promotes intestinal cancer progression in part by inducing IL-1β release.

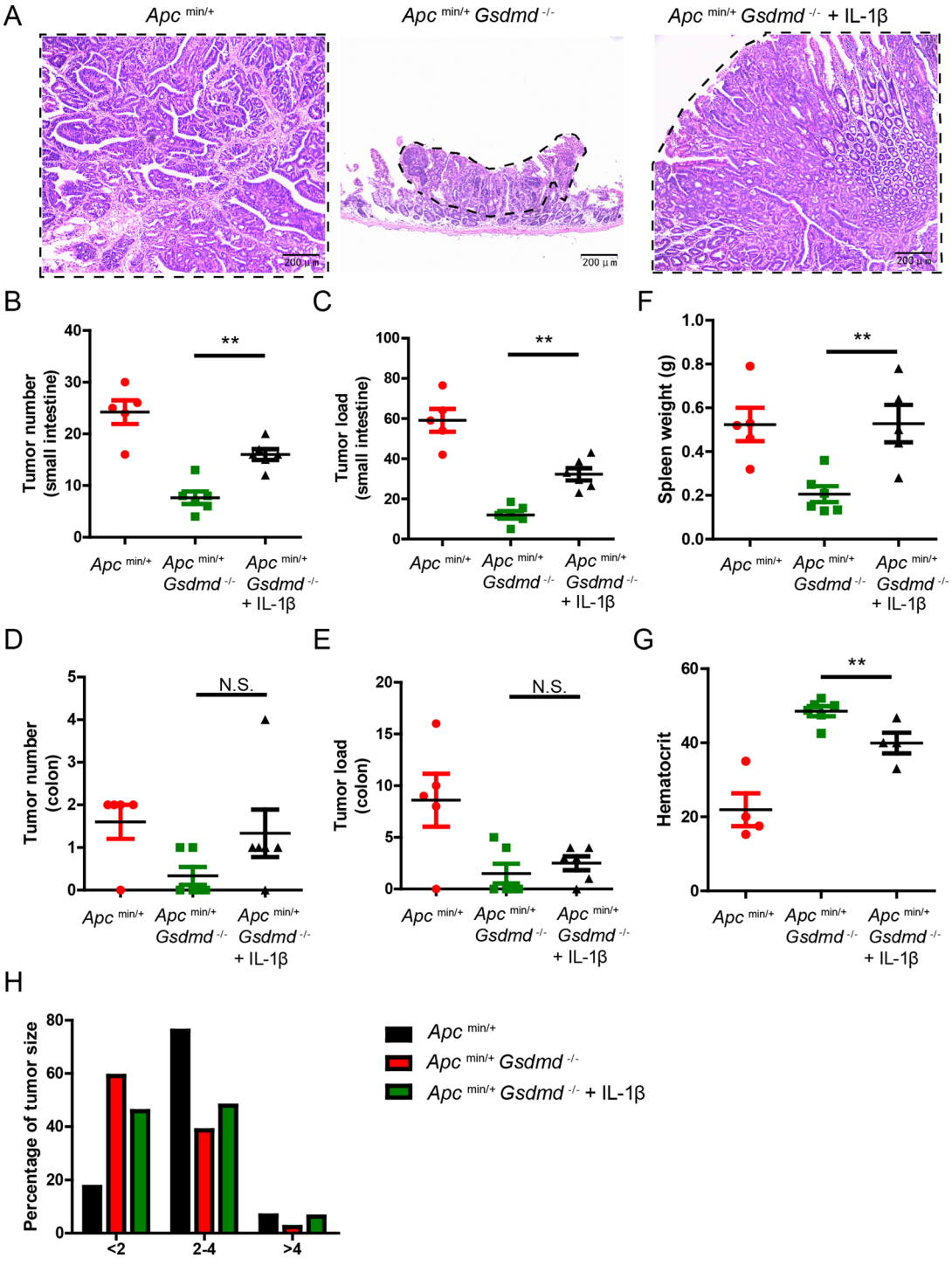

Fig. 4 Exogenous IL-1β promotes intestinal tumor development in $Apc^{min/+}Gsdmd^{-/-}$ mice. (**A**) 8-week-old $Apc^{min/+}Gsdmd^{-/-}$ mice simultaneously received injection of IL-1β or PBS twice a week, while age and sex-matched $Apc^{min/+}$ mice were injected with PBS ($n = 5$–6/group). H&E staining of the representative intestinal tumor from the 20-week old above mice (100× magnification). Tumors are circled with dashed lines. (**B**-**E**) Tumor number (**B** and **D**) and tumor load (**C** and **E**) from the small intestines or colons of 20-week-old above mice as in (**A**). (**F**-**G**) Spleen weight (**F**), and hematocrit (**G**) of 20-week-old above mice as in (**A**). (**H**) Histogram showing the size distribution of tumors from the small intestines of 20-week-old above mice as in (**A**). Data are representative of at least three independent experiments (mean ± SEM). $^{**}p < 0.01$ by Student's t test. N.S. means no significance

Apc$^{min/+}$*Gsdmd*$^{-/-}$ mice exhibit increased *Lactobacillus* abundance

Previous studies have shown that gene modifications can alter the composition of the gut microbiota in mice, and some of these alterations are associated with intestinal cancer development [5]. To investigate the differences in the gut microbiota between *Apc*$^{min/+}$ mice and *Apc*$^{min/+}$*Gsdmd*$^{-/-}$ mice, we performed 16S ribosomal RNA gene sequencing on fecal samples. A Venn diagram indicated that *Apc*$^{min/+}$ mice had 2,058 specific operational taxonomic units (OTUs), while *Apc*$^{min/+}$*Gsdmd*$^{-/-}$ mice had 1,230 specific OTUs, with 1,125 OTUs shared between both groups (Fig. 5A). The Simpson index revealed altered alpha diversity in

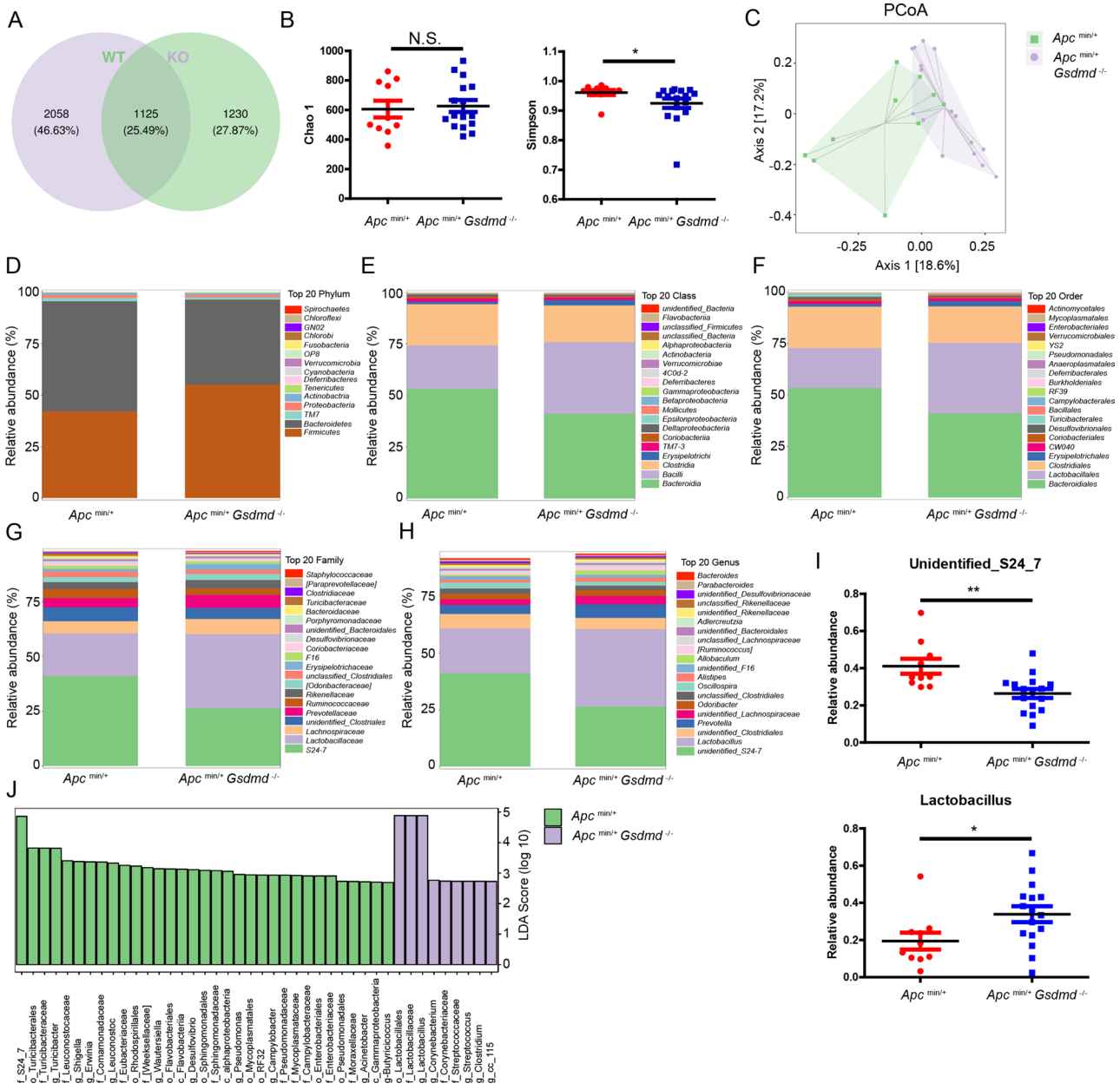

Fig. 5 Deficiency of GSDMD alters gut microbiota composition of *Apc*$^{min/+}$ mice. (**A**) Gut microbiota composition of fecal samples from 10-week-old *Apc*$^{min/+}$ ($n=10$) and *Apc*$^{min/+}$*Gsdmd*$^{-/-}$ ($n=16$) mice were assessed with 16S rRNA sequencing. Venn diagram of 16S rRNA sequencing data. WT means *Apc*$^{min/+}$ mice; KO means *Apc*$^{min/+}$*Gsdmd*$^{-/-}$ mice. (**B**) Chao 1 and Simpson index of 16S rRNA sequencing data as in (**A**). (**C**) PCoA analysis of 16S rRNA sequencing data as in (**A**). (**D-H**) Relative abundance of top 20 phylum (**D**), class (**E**), order (**F**), family (**G**), and genus (**H**) from the gut microbiota of *Apc*$^{min/+}$ ($n=10$) and *Apc*$^{min/+}$*Gsdmd*$^{-/-}$ ($n=16$) mice. (**I**) Relative abundance of *unidentified_S24_7* and *Lactobacillus* from the gut microbiota of *Apc*$^{min/+}$ ($n=10$) and *Apc*$^{min/+}$*Gsdmd*$^{-/-}$ ($n=16$) mice. (**J**) LEfSe analysis of the relative abundance from the gut microbiota of *Apc*$^{min/+}$ ($n=10$) and *Apc*$^{min/+}$*Gsdmd*$^{-/-}$ ($n=16$) mice. Data are representative of at least three independent experiments (mean ± SEM). *$p<0.05$, **$p<0.01$ by Student's t test

Apc$^{min/+}$*Gsdmd*$^{-/-}$ mice compared to *Apc*$^{min/+}$ mice, although the Chao 1 index was similar between the two groups (Fig. 5B). The community structure of the fecal microbiota also differed markedly between *Apc*$^{min/+}$*Gsdmd*$^{-/-}$ mice and *Apc*$^{min/+}$ mice (Fig. 5C). A heatmap illustrated differences in the gut microbiota composition between the two groups (Figure S2), which were further analyzed at the phylum, class, order, family, and genus levels (Fig. 5D-I). At the phylum level, *Firmicutes* were significantly increased, while *Bacteroidetes* were decreased in *Apc*$^{min/+}$*Gsdmd*$^{-/-}$ mice compared to *Apc*$^{min/+}$ mice (Fig. 5D). Consistent with these changes, *Bacilli* (class level), *Lactobacillales* (order level), *Lactobacillaceae* (family level), and *Lactobacillus* (genus level) were significantly enriched in *Apc*$^{min/+}$*Gsdmd*$^{-/-}$ mice, while *Bacteroidia* (class level), *Bacteroidiales* (order level), and *Lachnospiraceae* (family level) were reduced (Fig. 5E- G). At the genus level, *Apc*$^{min/+}$*Gsdmd*$^{-/-}$ mice exhibited significantly higher levels of *Lactobacillus* compared to *Apc*$^{min/+}$ mice (Fig. 5H and I). Linear discriminant analysis effect size (LEfSe) further confirmed the enrichment of *Lactobacillales*, *Lactobacillaceae*, and *Lactobacillus* in *Apc*$^{min/+}$*Gsdmd*$^{-/-}$ mice (Fig. 5J). These findings suggest that GSDMD deficiency alters the gut microbiota composition, as *Apc*$^{min/+}$*Gsdmd*$^{-/-}$ mice display an increased abundance of *Lactobacillus*.

Apc$^{min/+}$*Gsdmd*$^{-/-}$ mice exhibit reduced kynurenine levels

To determine whether changes in the microbiota composition contribute to intestinal tumor development of *Apc*$^{min/+}$*Gsdmd*$^{-/-}$ mice through microbiota-associated metabolites, we further investigated the metabolites in the feces of *Apc*$^{min/+}$*Gsdmd*$^{-/-}$ mice and *Apc*$^{min/+}$ mice using mass spectrometry. Partial least squares discriminant analysis (PLS-DA) revealed distinct metabolomic profiles between *Apc*$^{min/+}$*Gsdmd*$^{-/-}$ mice and *Apc*$^{min/+}$ mice (Fig. 6A). A total of 781 metabolites were identified in the feces, with 25 downregulated metabolites and 61 upregulated metabolites in *Apc*$^{min/+}$ mice compared to *Apc*$^{min/+}$*Gsdmd*$^{-/-}$ mice (Fig. 6B). The upregulated metabolites (Fig. 6C) and downregulated metaboiltes (Figure S3) were showed using heatmaps. The correlation of different metaboiltes was showed with correlated heatmap (Figure S4). Z-score analysis highlighted significant differences in metabolite abundance, with L-Kynurenine (Kyn) being particularly elevated (Fig. 6D). Kyoto Encyclopedia of Genes and Genomes (KEGG) pathway analysis identified tryptophan (Trp) metabolism as the pathway most affected by GSDMD deficiency (Fig. 6E). A network diagram revealed that Kyn, indolepyruvate, quinolinic acid, and 3-methoxyanthranilate were elevated, while 3-hydroxyanthranilate and 2-aminobenzoic acid were reduced in *Apc*$^{min/+}$ mice compared to *Apc*$^{min/+}$*Gsdmd*$^{-/-}$ mice (Fig. 6F), which was confirmed by intensity analysis (Fig. 6G). Kyn has been implicated in intestinal cancer development [21, 22], and its reduction in *Apc*$^{min/+}$*Gsdmd*$^{-/-}$ mice may contribute to the reduced tumor formation observed in these animals.

Kynurenine levels negatively correlate with *Lactobacillus* abundance

To determine the correlation of microbiota and metabolites, correlated heatmap was carried out with Pearson correlation analysis. We found that Kyn was positively correlated with *Bacteroidia* (class level) and negatively correlated with *Bacilli* (class level) (Figure S5A). Consistent with the class level, Kyn was positively correlated with *Bacteroidiales* (order level), *Lachnospiraceae* (family level), and *unidentified_S24-7*, but negatively correlated with *Lactobacillales* (order level), *Lactobacillaceae* (family level), and *Lactobacillus* (genus level) (Figure S5B-5D). Correlation scatter plots showed that fecal microbiota from *Apc*$^{min/+}$*Gsdmd*$^{-/-}$ mice had more *Bacilli* (class level) and fewer *Bacteroidia* (class level), which were negatively and positively correlated with Kyn respectively (Figure S5E). These trends were consistent across the order, family, and genus levels (Figure S5F-5H). The data suggest that increased *Lactobacillus* may promote intestinal tumor formation through suppressing Kyn production in *Apc*$^{min/+}$*Gsdmd*$^{-/-}$ mice.

Exogenous kynurenine promotes colon cancer development in *Apc*$^{min/+}$*Gsdmd*$^{-/-}$ mice

We observed reduced Kyn in the feces of *Apc*$^{min/+}$*Gsdmd*$^{-/-}$ mice. As is known, Kyn is a metabolite derived from Trp metabolism, which includes endogenous (host) Trp metabolism and bacterial Trp metabolism. Kyn is produced by endogenous Trp metabolism, but not by bacterial Trp metabolism [28]. To confirm this in our setting, we measured Kyn and Trp levels in the colon tissues of mice. Consistent with a previous report [22], we found that *Apc*$^{min/+}$*Gsdmd*$^{-/-}$ mice exhibited lower Kyn but not Trp levels in colon tissue compared to *Apc*$^{min/+}$ mice (Fig. 7A). The ratio of Kyn/Trp was significantly reduced in the colon of *Apc*$^{min/+}$ mice (Fig. 7B). To determine whether reduced tumor formation in *Apc*$^{min/+}$*Gsdmd*$^{-/-}$ mice was due to lower Kyn levels, we intraperitoneally injected Kyn into 8-week-old *Apc*$^{min/+}$*Gsdmd*$^{-/-}$ mice and analyzed tumor development after 12 weeks. We found that the administration of exogenous Kyn increased Kyn levels in the serum and feces of *Apc*$^{min/+}$*Gsdmd*$^{-/-}$ mice (Figure S6). As expected, exogenous Kyn significantly increased tumor size in the small intestines of *Apc*$^{min/+}$*Gsdmd*$^{-/-}$ mice (Fig. 7C). Additionally, Kyn-treated *Apc*$^{min/+}$*Gsdmd*$^{-/-}$ mice exhibited an increased tumor number (Fig. 7D and F) and tumor load (Fig. 7E and G) in both the small intestine and colon. Meanwhile, Kyn increased spleen weight (Fig. 7H)

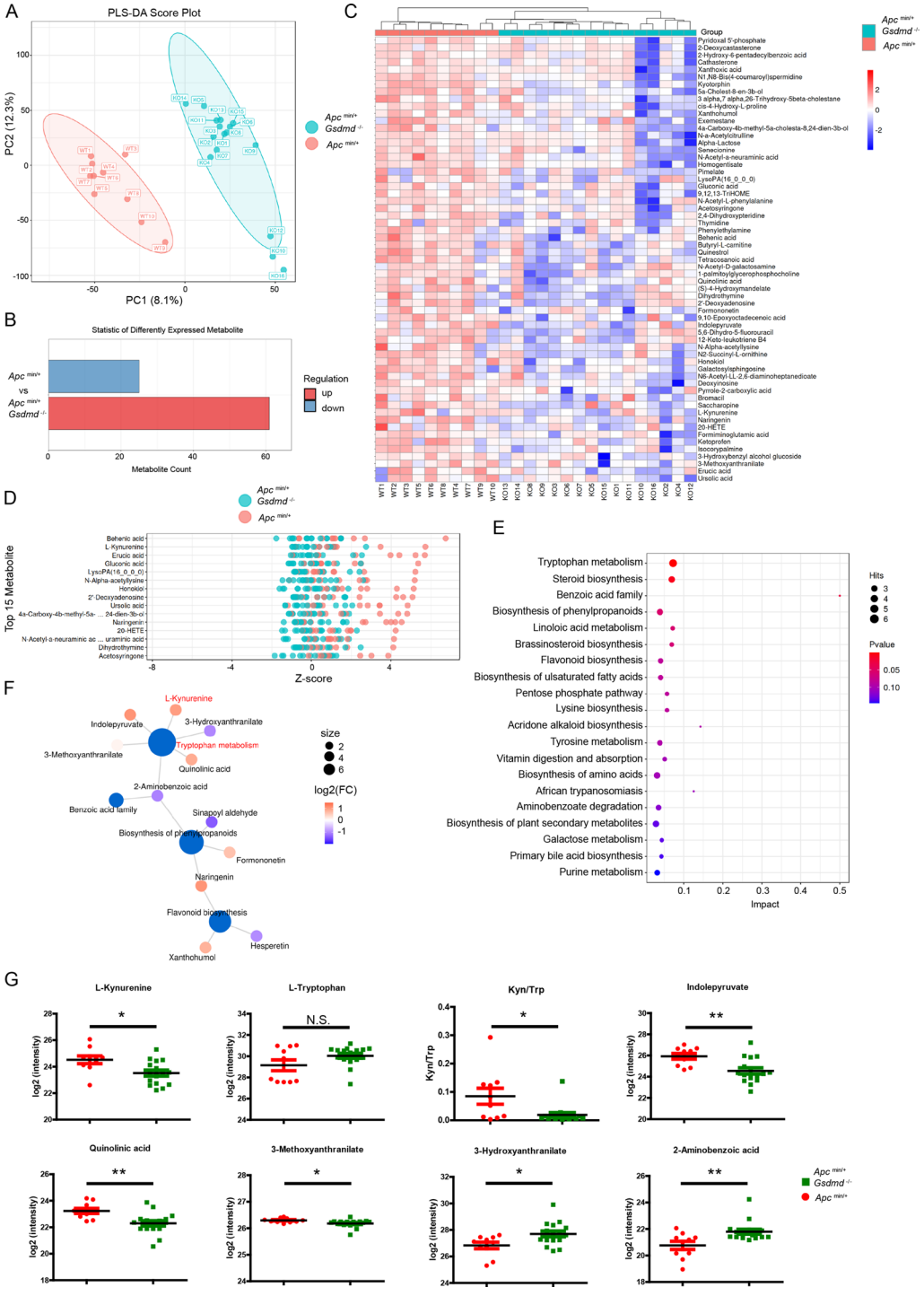

Fig. 6 Deficiency of GSDMD alters gut metabolites of $Apc^{min/+}$ mice. (**A**) PLS-DA scores for fecal metabolites of $Apc^{min/+}$ ($n=10$) and $Apc^{min/+}Gsdmd^{-/-}$ ($n=16$) mice. (**B**) Statistics of differentially expressed fecal metabolites in $Apc^{min/+}$ ($n=10$) and $Apc^{min/+}Gsdmd^{-/-}$ ($n=16$) mice. (**C**) Heatmap analysis of upregulated metabolites in $Apc^{min/+}$ ($n=10$) mice compared to $Apc^{min/+}Gsdmd^{-/-}$ ($n=16$) mice. WT means $Apc^{min/+}$ mice; KO means $Apc^{min/+}Gsdmd^{-/-}$ mice. (**D**) Top 15 metabolites of $Apc^{min/+}$ ($n=10$) and $Apc^{min/+}Gsdmd^{-/-}$ ($n=16$) mice based on Z-score. (**E**) Top 20 enriched KEGG pathways of differentially expressed fecal metabolites in $Apc^{min/+}$ ($n=10$) and $Apc^{min/+}Gsdmd^{-/-}$ ($n=16$) mice. (**F**) Network of KEGG enriched pathway. Blue dot: pathway, red dot: upregulated metabolite, purple dot: downregulated metabolite. Metabolites from $Apc^{min/+}$ mice vs. metabolites from $Apc^{min/+}Gsdmd^{-/-}$ mice. (**G**) Log2(intensity) of Trp pathway metabolites in $Apc^{min/+}$ ($n=10$) and $Apc^{min/+}Gsdmd^{-/-}$ ($n=16$) mice. Data are representative of at least three independent experiments (mean ± SEM). $^{*}p<0.05$, $^{**}p<0.01$ by Student's t test. N.S. means no significance

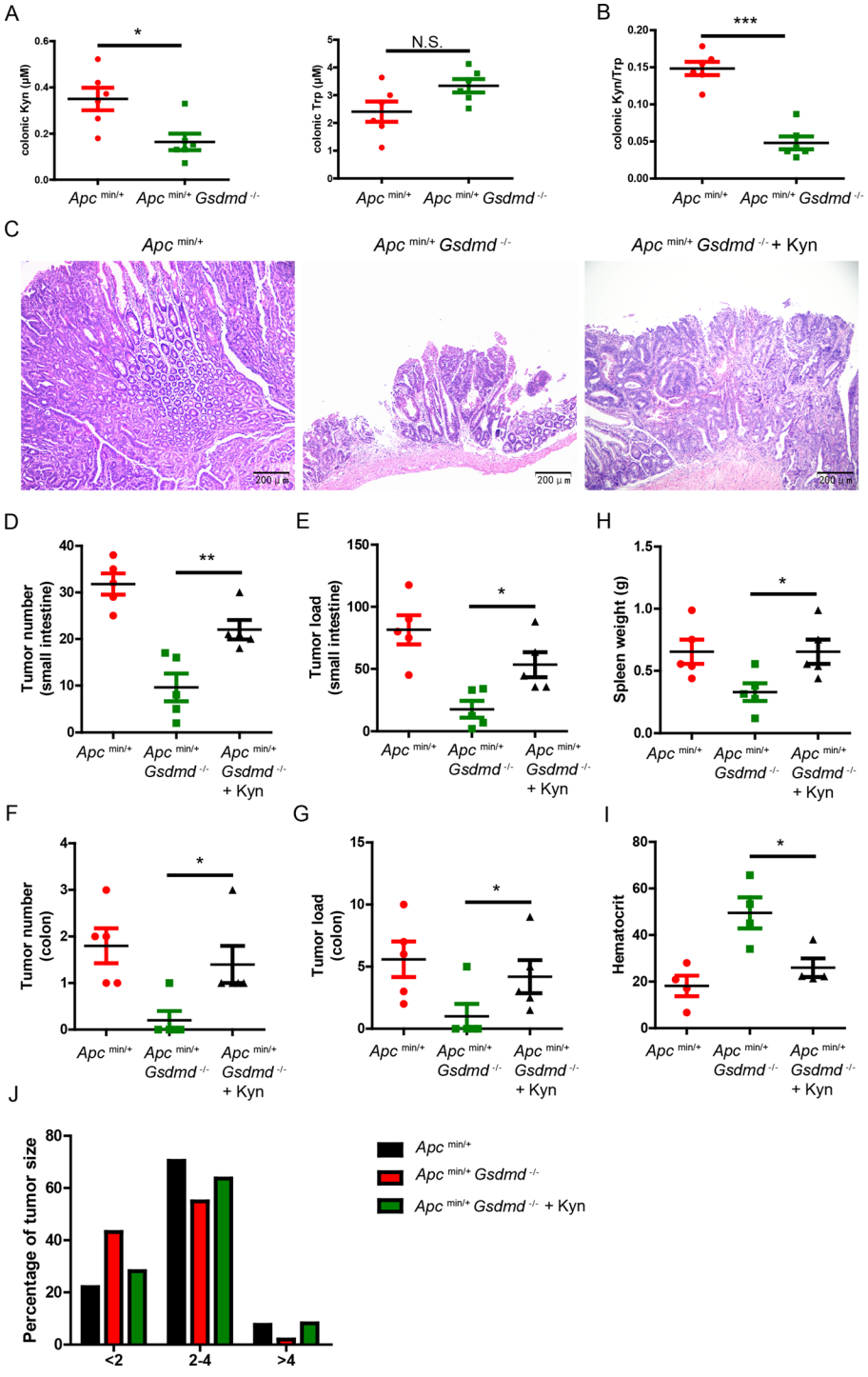

Fig. 7 Exogenous Kyn promotes intestinal tumor development in *Apc*$^{min/+}$*Gsdmd*$^{-/-}$ mice. (**A**) ELISA analysis of Kyn and Trp from colon of *Apc*$^{min/+}$ ($n=6$) and *Apc*$^{min/+}$*Gsdmd*$^{-/-}$ ($n=6$) mice. (**B**) Kyn/Trp was determined as in (**A**). (**C**) 8-week-old *Apc*$^{min/+}$*Gsdmd*$^{-/-}$ mice simultaneously received injection of Kyn or PBS once a week, while age and sex-matched *Apc*$^{min/+}$ mice were injected with PBS ($n=5$/group). H&E staining of the representative intestinal tumor from the 20-week old above mice (100× magnification). (**D**-**G**) Tumor number (**D** and **F**) and tumor load (**E** and **G**) from the small intestines or colons of 20-week-old above mice as in (**C**). (**H**-**I**) Spleen weight (**H**), and hematocrit (**I**) of 20-week-old above mice as in (**C**). (**J**) Histogram showing the size distribution of tumors from the small intestines of 20-week-old above mice as in (**C**). Data are representative of at least three independent experiments (mean ± SEM). *$p<0.05$, **$p<0.01$, ***$p<0.001$ by Student's t test. N.S. means no significance

and exacerbated anemia (Fig. 7I) in $Apc^{min/+}Gsdmd^{-/-}$ mice. Tumor size distribution analysis further indicated that exogenous Kyn increased tumor size in $Apc^{min/+}Gsdmd^{-/-}$ mice (Fig. 7J). These results suggest that exogenous Kyn partially restores intestinal tumor formation in $Apc^{min/+}Gsdmd^{-/-}$ mice.

Kyn is known to promote colon cancer by reducing $CD8^+$ T cell numbers and increasing regulatory T (Treg) cell numbers [22, 24]. In $Apc^{min/+}Gsdmd^{-/-}$ mice, $CD8^+$ T cell numbers were higher in intestinal tumors, and exogenous Kyn reduced these numbers (Fig. 8A and B). Treg cells, which were reduced in $Apc^{min/+}Gsdmd^{-/-}$ mice, were increased by Kyn treatment (Fig. 8C and D). These data suggest that Kyn promotes tumor development in $Apc^{min/+}Gsdmd^{-/-}$ mice, likely by enhancing immunosuppression.

Discussion

The interaction between gut microbiota and the host plays a pivotal role in maintaining gut homeostasis. Gut microbiota is critically involved in the development of colitis and colorectal cancer (CRC). However, the molecular mechanisms by which gut microbiota mediates CRC progression remain largely unexplored. In this study, we demonstrate that GSDMD promotes intestinal tumor development by increasing IL-1β release and Kyn production, and GSDMD increases Kyn production might through suppressing *Lactobacillus* abundance in the gut.

GSDMD is a key executor of the inflammasome, responsible for the release of mature IL-1β and IL-18, as well as mediating pyroptotic cell death [6]. It has been reported that GSDMD sensitized colorectal cancer to chemotherapy in pyroptosis dependent and independent manner [18, 29]. A recent paper reported that GSDMD suppressed inflammation-induced colon cancer by promoting STAT1-dependent apoptosis in azomethanze plus dextran sulfate sodium-induced CRC mice model [19]. In contrast, another paper found that a point mutation in leucine-rich repeat kinase 2 (LRRK2 G2019S) promoted colon cancer progression via LRRK2-GSDMD mediated gut inflammation in the same model [20]. These findings suggest that the role of GSDMD in inflammation-associated colon cancer is complex and context-dependent. In our study, we investigated the role of GSDMD in spontaneous colon cancer development using $Apc^{min/+}$ mice, a widely used model for CRC. We found that GSDMD deficiency reduced spontaneous intestinal tumor development, likely through modulation of IL-1β release and Kyn production. While previous studies reported decreased GSDMD expression in human colon cancer tissues compared to peritumoral tissues [19, 29], we observed that GSDMD expression was significantly higher in colon cancer tissues than in adjacent non-tumor tissues. Additionally, GSDMD expression positively correlated with tumor grade and tumor size. Differences in patient specimens, antibodies, and experimental conditions may account for these seemingly contradictory results. Larger studies involving more patient samples are required to confirm GSDMD protein levels in CRC.

It is well-established that IL-1β is an effector cytokine produced by activated inflammasomes and promotes colon cancer development through various mechanisms, including enhancing tumor cell proliferation and modulating the tumor microenvironment [9–12]. Consistent with a previous report [30], we observed that IL-1β mRNA levels were comparable between $Apc^{min/+}$ mice and $Apc^{min/+}Gsdmd^{-/-}$ mice. However, the protein level of IL-1β was significantly elevated in $Apc^{min/+}$ mice and reduced in $Apc^{min/+}Gsdmd^{-/-}$ mice. These results suggest that GSDMD promotes IL-1β release in $Apc^{min/+}$ mice. Furthermore, we found exogenous recombinant IL-1β partially rescued intestinal tumor development in $Apc^{min/+}Gsdmd^{-/-}$ mice. However, IL-1β produced by which type of cell in $Apc^{min/+}$ mice still remains unclear, and we speculated that IL-1β may be produced by myeloid cells. To answer the question, future studies should utilize tissue- or cell-specific *Gsdmd* knockout mice, generated through the Cre/LoxP recombination system, to elucidate the cellular sources of IL-1β [31].

Previous work from our group showed that $Gsdmd^{-/-}$ mice exhibited reduced levels of intestinal *Firmicutes* and no change in *Lactobacillus* levels compared to controls [26]. However, in the present study, we observed an increase in *Firmicutes* and a decrease in *Bacteroidetes* in $Apc^{min/+}Gsdmd^{-/-}$ mice compared to $Apc^{min/+}$ mice. Consistent with the changes in phylum level, *Bacilli* (class level), *Lactobacillales* (order level), *Lactobacillaceae* (family level), and *Lactobacillus* (genus level) significantly increased in the gut of $Apc^{min/+}Gsdmd^{-/-}$ mice. The data suggest that GSDMD may increase *Firmicutes* levels under normal condition, while it may decrease *Firmicutes* levels during spontaneous intestinal cancer development. This indicates that GSDMD has varying effects on gut microbiota composition under different physiological and pathological conditions.

Trp metabolism consists of endogenous (host) and bacterial pathways [28]. Kyn is a key metabolite derived from endogenous Trp metabolism but not bacterial Trp metabolism. Indoleamine 2,3-dioxygenase (IDO) is a critical enzyme for digesting Trp to Kyn [25]. Kyn is considered to be an oncometabolite in CRC [21]. In our study, we observed a marked reduction in Kyn levels in the feces of $Apc^{min/+}Gsdmd^{-/-}$ mice. Moreover, exogenous Kyn promoted intestinal tumor development in these mice, demonstrating that Kyn is crucial for spontaneous intestinal tumor progression. Interestingly, we found a strong inverse correlation between Kyn levels and *Lactobacillus* abundance. A previous report found that colonization

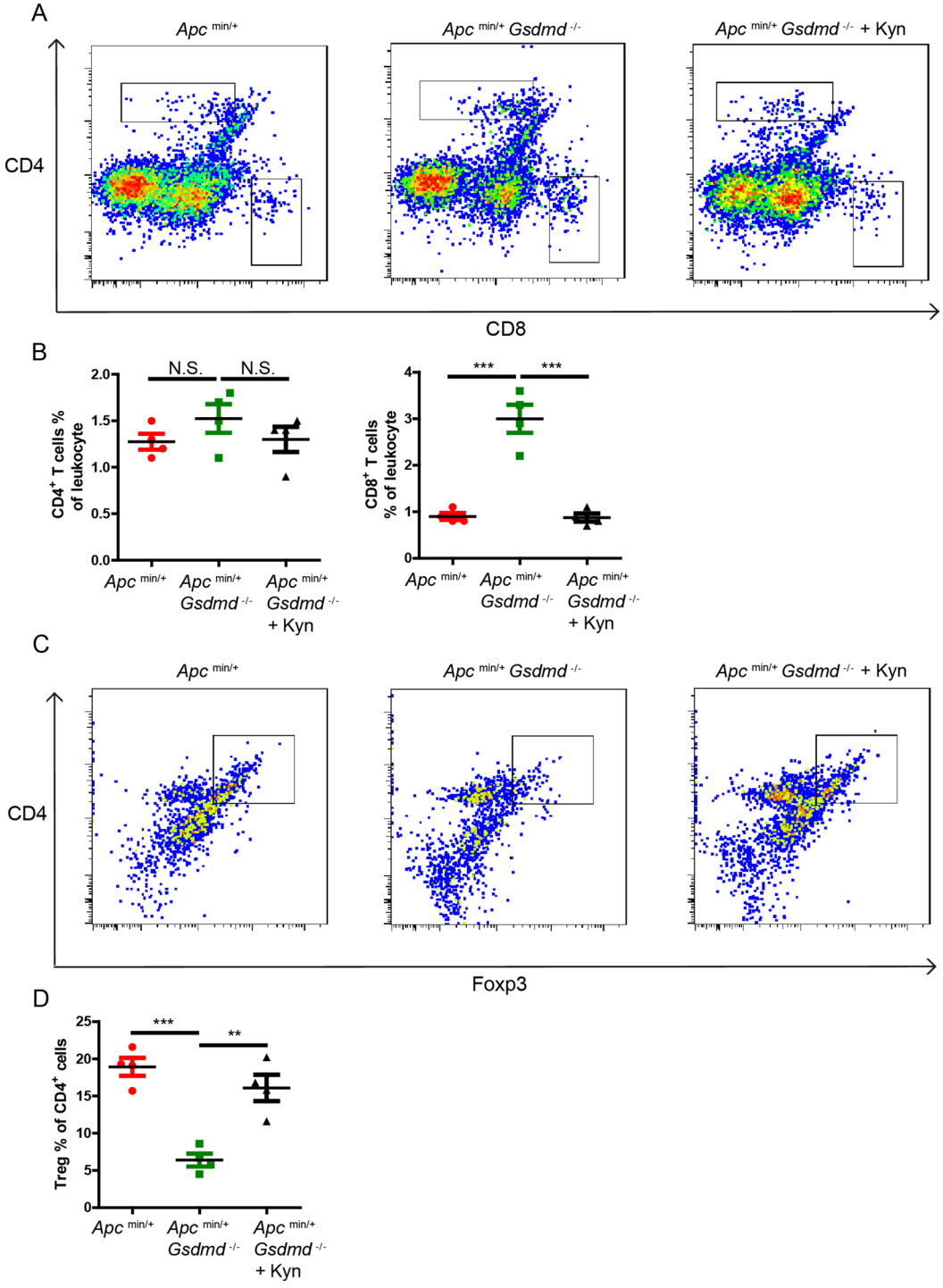

Fig. 8 Exogenous Kyn increases Treg cell number in *Apc*$^{min/+}$*Gsdmd*$^{-/-}$ mice. (**A**) 8-week-old *Apc*$^{min/+}$*Gsdmd*$^{-/-}$ mice simultaneously received injection of Kyn or PBS once a week, while age and sex-matched *Apc*$^{min/+}$ mice were injected with PBS ($n = 4$/group). Flow cytometry analysis of CD4$^+$ and CD8$^+$ T cell number from intestinal tumor of the 20-week old above mice. (**B**) Total leukocytes were determined by CD45$^+$ cell. CD4$^+$ T cells % of total leukocyte and CD8$^+$ T cells % of total leukocyte were determined as in (**A**). (**C**) Flow cytometry analysis of Treg (CD4$^+$ Foxp3$^+$) cell number from intestinal tumor of the 20-week old mice as in (**A**). (**D**) Treg % of CD4$^+$ cells was determined as in (**C**). Data are representative of at least three independent experiments (mean ± SEM). $^{**}p < 0.01$, $^{***}p < 0.001$ by Student's t test. N.S. means no significance

with *Lactobacillus johnsonii* in rats decreased serum Kyn levels [32]. *L.johnsonii* reduced IDO1 activity in HT-29 cells, a human colon cancer cell line [33]. Based on these observations, we propose that *Lactobacillus* may suppress endogenous Trp metabolism in $Apc^{min/+}Gsdmd^{-/-}$ mice. To test this hypothesis, future studies need to be investigated whether *Lactobacillus* transplantation into SPF wild-type C57/BL6 or germ-free mice can suppress endogenous Trp metabolism. Additionally, it would be of interest to explore whether Kyn itself influences gut microbiota composition.

In conclusion, our study identifies GSDMD as a key promoter of colon cancer development, likely through enhancing IL-1β release and Kyn production. We propose that GSDMD serves as a critical link between the host and gut microbiota, and GSDMD-mediated suppression of *Lactobacillus* abundance may enhance Kyn production from host cells. Therefore, targeting GSDMD represents a promising therapeutic strategy for CRC.

Supplementary Information

The online version contains supplementary material available at https://doi.org/10.1186/s12964-024-01890-6.

Supplementary Material 1

Acknowledgements
Not applicable.

Author contributions
Hanchao Gao, Mengtao Cao, and Pengfei Chen designed the experiments. Hanchao Gao and Pengfei Chen wrote the manuscript. Hanchao Gao, Weilong Li, and Shi Xu conducted the experiments and analyzed the data. Zigan Xu, Wenjun Hu, Litao Pan, Ting Xie, Yeye Yu, Huimin Sun, Liwen Huang, Peishan Chen, Jinmei Wu, Dexing Yang and Lian Li helped with experiments. Litao Pan, and Kewang Luo provided reagents and technical support. Hanchao Gao and Shaodong Luan supervised the study. All authors reviewed and approved the submitted version.

Funding
This work was supported by grants from Guangdong Basic and Applied Basic Research Foundation (2024A1515030207), Open Project of Guangdong Provincial Key Laboratory of Tropical Disease Research (KLTDR202002), Shenzhen Foundation of Science and Technology (JCYJ20220531092614032, JCYJ20220531092617039), Shenzhen Longhua District Science and Technology Innovation Special Fund Project (11501A20220923BF59236, 11501A20220923BE5B6B3, 11501A20220923BD5F291).

Data availability
The datasets generated and/or analyzed during the current study are available in the National Center for Biotechnology Information repository (no. PRJNA1109541; https://www.ncbi.nlm.nih.gov/bioproject/PRJNA1109541).

Declarations

Ethics approval and consent to participate
The animal study was reviewed and approved by Institutional Biomedical Research Ethics Committee of the Guangdong Medical University.

Consent for publication
All the authors give their consent for publication.

Competing interests
The authors declare no competing interests.

Author details
[1]Department of Nephrology, Shenzhen Longhua District Key Laboratory for Diagnosis and Treatment of Chronic Kidney Disease, Shenzhen Longhua District Central Hospital, Shenzhen, Guangdong 518110, China
[2]Department of Burn and Plastic Surgery, Shenzhen Longhua District Central Hospital, Shenzhen, Guangdong 518110, China
[3]Department of Anesthesiology, The 305 Hospital of Liberation Army of China (PLA), Beijing 100036, China
[4]Department of Acupuncture and Massage, Shenzhen Second People's Hospital, The First Affiliated Hospital of Shenzhen University, Shenzhen, Guangdong 518037, China
[5]Department of Medical Laboratory, People's Hospital of Longhua, Shenzhen, Guangdong 518110, China
[6]Department of Nephrology, The First Affiliated Hospital of Jinan University, Guangzhou, Guangdong 510632, China
[7]Wuzhou Medical College, Wuzhou, Guangxi 543199, China
[8]Department of Respiratory Medicine, Shenzhen Longhua District Central Hospital, Shenzhen, Guangdong 518110, China
[9]Department of Traumatic Orthopedics, Shenzhen Longhua District Central Hospital, Shenzhen, Guangdong 518110, China

Received: 13 May 2024 / Accepted: 11 October 2024
Published online: 21 October 2024

References

1. Schmitt M, Greten FR. The inflammatory pathogenesis of colorectal cancer. Nat Rev Immunol. 2021;21:653–67.
2. Okayasu I, Ohkusa T, Kajiura K, Kanno J, Sakamoto S. Promotion of colorectal neoplasia in experimental murine ulcerative colitis. Gut. 1996;39:87–92.
3. Rakoff-Nahoum S, Medzhitov R. Regulation of spontaneous intestinal tumorigenesis through the adaptor protein MyD88. Science. 2007;317:124–7.
4. Penny HL, Prestwood TR, Bhattacharya N, Sun F, Kenkel JA, Davidson MG, Shen L, Zuniga LA, Seeley ES, Pai R, Choi O, Tolentino L, Wang J, Napoli JL. Engleman, restoring retinoic acid attenuates intestinal inflammation and Tumorigenesis in APCMin/+ mice. Cancer Immunol Res. 2016;4:917–26.
5. Wong CC, Yu J. Gut microbiota in colorectal cancer development and therapy. Nat Rev Clin Oncol. 2023;20:429–52.
6. Elias EE, Lyons B, Muruve DA. Gasdermins and pyroptosis in the kidney. Nat Rev Nephrol. 2023;19:337–50.
7. Wei X, Xie F, Zhou X, Wu Y, Yan H, Liu T, Huang J, Wang F, Zhou F, Zhang L. Role of pyroptosis in inflammation and cancer. Cell Mol Immunol. 2022;19:971–92.
8. Sharma BR, Kanneganti TD. Inflammasome signaling in colorectal cancer. Transl Res. 2023;252:45–52.
9. Li Y, Wang L, Pappan L, Galliher-Beckley A, Shi J. IL-1beta promotes stemness and invasiveness of colon cancer cells through Zeb1 activation. Mol Cancer. 2012;11:87.
10. Rebe C, Ghiringhelli F. Interleukin-1beta and Cancer. Cancers (Basel). 2020;12(7).
11. Zhu Y, Zhu M, Lance P. IL1beta-mediated stromal COX-2 signaling mediates proliferation and invasiveness of colonic epithelial cancer cells. Exp Cell Res. 2012;318:2520–30.
12. Voronov E, Apte RN. IL-1 in Colon inflammation, Colon carcinogenesis and invasiveness of Colon cancer. Cancer Microenviron. 2015;8:187–200.
13. Shi J, Zhao Y, Wang K, Shi X, Wang Y, Huang H, Zhuang Y, Cai T, Wang F, Shao F. Cleavage of GSDMD by inflammatory caspases determines pyroptotic cell death. Nature. 2015;526:660–5.
14. Liu X, Zhang Z, Ruan J, Pan Y, Magupalli VG, Wu H, Lieberman J. Inflammasome-activated gasdermin D causes pyroptosis by forming membrane pores. Nature. 2016;535:153–8.
15. Kuang S, Zheng J, Yang H, Li S, Duan S, Shen Y, Ji C, Gan J, Xu XW, Li J. Structure insight of GSDMD reveals the basis of GSDMD autoinhibition in cell pyroptosis. Proc Natl Acad Sci U S A. 2017;114:10642–7.
16. Vasudevan SO, Behl B, Rathinam VA. Pyroptosis-induced inflammation and tissue damage. Semin Immunol. 2023;69:101781.
17. Wang S, Chang CW, Huang J, Zeng S, Zhang X, Hung MC, Hou J. Gasdermin C sensitizes tumor cells to PARP inhibitor therapy in cancer models. J Clin Invest. 2024;134(1).

18. Wu LS, Liu Y, Wang XW, Xu B, Lin YL, Song Y, Dong Y, Liu JL, Wang XJ, Liu S, Kong P, Han M, Li BH. LPS enhances the chemosensitivity of oxaliplatin in HT29 cells via GSDMD-Mediated pyroptosis. Cancer Manag Res. 2020;12:10397–409.
19. Tanaka S, Orita H, Kataoka T, Miyazaki M, Saeki H, Wada R, Brock MV, Fukunaga T, Amano T, Shiroishi T. Gasdermin D represses inflammation-induced colon cancer development by regulating apoptosis. Carcinogenesis. 2023;44:341–9.
20. Wang Y, Gao JZ, Sakaguchi T, Maretzky T, Gurung P, Narayanan NS, Short S, Xiong Y, Kang Z. LRRK2 G2019S Promotes Colon Cancer Potentially via LRRK2-GSDMD Axis-Mediated Gut Inflammation. Cells. 2024;13(7).
21. Venkateswaran N, Conacci-Sorrell M. Kynurenine: an oncometabolite in colon cancer. Cell Stress. 2020;4:24–6.
22. Zhang X, Liu X, Zhou W, Du Q, Yang M, Ding Y, Hu R. Blockade of IDO-Kynurenine-AhR Axis ameliorated Colitis-Associated Colon Cancer via Inhibiting Immune Tolerance. Cell Mol Gastroenterol Hepatol. 2021;12:1179–99.
23. Venkateswaran N, Lafita-Navarro MC, Hao YH, Kilgore JA, Perez-Castro L, Braverman J, Borenstein-Auerbach N, Kim M, Lesner NP, Mishra P, Brabletz T, Shay JW, DeBerardinis RJ, Williams NS, Yilmaz OH, Conacci-Sorrell M. MYC promotes tryptophan uptake and metabolism by the kynurenine pathway in colon cancer. Genes Dev. 2019;33:1236–51.
24. Wu D, Zhu Y. Role of kynurenine in promoting the generation of exhausted CD8(+) T cells in colorectal cancer. Am J Transl Res. 2021;13:1535–47.
25. Bishnupuri KS, Alvarado DM, Khouri AN, Shabsovich M, Chen B, Dieckgraefe BK, Ciorba MA. IDO1 and kynurenine pathway metabolites activate PI3K-Akt signaling in the neoplastic Colon epithelium to Promote Cancer Cell Proliferation and inhibit apoptosis. Cancer Res. 2019;79:1138–50.
26. Gao H, Cao M, Yao Y, Hu W, Sun H, Zhang Y, Zeng C, Tang J, Luan S, Chen P. Dysregulated microbiota-driven gasdermin D activation promotes Colitis Development by mediating IL-18 release. Front Immunol. 2021;12:750841.
27. Song X, Gao H, Lin Y, Yao Y, Zhu S, Wang J, Liu Y, Yao X, Meng G, Shen N, Shi Y, Iwakura Y, Qian Y. Alterations in the microbiota drive interleukin-17 C production from intestinal epithelial cells to promote tumorigenesis. Immunity. 2014;40:140–52.
28. Gao J, Xu K, Liu H, Liu G, Bai M, Peng C, Li T, Yin Y. Impact of the gut microbiota on intestinal immunity mediated by Tryptophan Metabolism. Front Cell Infect Microbiol. 2018;8:13.
29. Peng X, Na R, Zhou W, Meng X, Yang Y, Amini S, Song L. Nuclear translocation of gasdermin D sensitizes colorectal cancer to chemotherapy in a pyroptosis-independent manner. Oncogene. 2022;41:5092–106.
30. Dmitrieva-Posocco O, Dzutsev A, Posocco DF, Hou V, Yuan W, Thovarai V, Mufazalov IA, Gunzer M, Shilovskiy IP, Khaitov MR, Trinchieri G, Waisman A, Grivennikov SI. Cell-type-specific responses to Interleukin-1 Control Microbial Invasion and Tumor-elicited inflammation in Colorectal Cancer. Immunity. 2019;50:166–80. e167.
31. Lu ZY, Chen PB, Xu QY, Li B, Jiang SD, Jiang LS, Zheng XF. Constitutive and conditional gene knockout mice for the study of intervertebral disc degeneration: current status, decision considerations, and future possibilities. JOR Spine. 2023;6:e1242.
32. Valladares R, Bojilova L, Potts AH, Cameron E, Gardner C, Lorca G, Gonzalez CF. Lactobacillus johnsonii inhibits indoleamine 2,3-dioxygenase and alters tryptophan metabolite levels in BioBreeding rats. FASEB J. 2013;27:1711–20.
33. Freewan M, Rees MD, Plaza TS, Glaros E, Lim YJ, Wang XS, Yeung AW, Witting PK, Terentis AC, Thomas SR. Human indoleamine 2,3-dioxygenase is a catalyst of physiological heme peroxidase reactions: implications for the inhibition of dioxygenase activity by hydrogen peroxide. J Biol Chem. 2013;288:1548–67.

Publisher's note